Check for updates

Sub-meter resolution wetland map of Hainan with detailed types from multi-source satellite imagery

Xiaohai Zhang[1,2], Jiahui Liu[1]*, Sheng Liu[1], Jiaju Yu[3], Kang Deng[1], Weiping Ding[1], Zeheng Chen[1] and Fangyi Li[1]*

[1]Haikou Marine Geological Survey Center, China Geological Survey, Haikou, China, [2]The Haikou Key Laboratory of Marine Contaminants Monitoring Innovation and Application, Haikou, China, [3]School of Statistics and Data Science, Jiangxi University of Finance and Economics, Nanchang, China

Introduction: Obtaining wetland data with high spatial accuracy and typological completeness is essential for understanding ecosystem functions, evaluating services, and informing conservation policy. However, fine-scale wetland mapping in tropical island regions remains challenging due to persistent cloud cover, image limitations, complex wetland types, and dynamic hydrology.

Methods: We developed a sub-meter resolution wetland mapping framework for Hainan Island, China, by integrating multi-source optical imagery (WorldView-2/3, Gaofen-1/2), dual-temporal features, and RTK-based field validation. A hierarchical classification system was designed, consisting of three major categories and 17 subcategories, aligned with Ramsar Convention criteria and adapted to island-specific conditions.

Results: The 2019 wetland map (3842.84 km^2) achieved an overall accuracy of 96.13% (Kappa = 0.95). The framework successfully identified numerous small and fragmented wetland patches (0.0004−0.08 km^2) that had been omitted in national wetland inventories. The results also revealed rapid artificial wetland expansion and pronounced spatial heterogeneity in natural wetlands.

Discussion: This study delivers a reliable high-resolution dataset and a replicable methodology for tropical island wetland mapping. The results provide a critical basis for wetland monitoring, blue carbon assessment, and ecological management, while offering a transferable framework that can be applied to other coastal and island environments.

1 Introduction

Wetlands, often referred to as the "kidneys of the Earth," are among the most important habitats for humanity (Adamus, 2013; Bo et al., 2020; Geng et al., 2023). As one of the three major global ecosystems alongside forests and oceans, wetlands are multifunctional and highly biodiverse (Guo et al., 2017; Dang et al., 2021; Salimi et al., 2021). Wetlands play vital ecological and social roles, including maintaining biodiversity, controlling soil erosion,

regulating water cycles, purifying water, and modulating local climate (Poiani et al., 1996; Heimann et al., 1998; Mitsch et al., 2013; Hu et al., 2017; Xu et al., 2020; Zhu et al., 2022).

Although wetlands contribute an estimated 25% of global methane emissions (Whalen, 2005; Igwe et al., 2022), their high carbon sequestration capacity and the relatively short atmospheric lifetime of methane render them net carbon sinks (Mitsch et al., 2013), making wetlands critical to the global carbon cycle.

However, wetlands rank among the most vulnerable and rapidly declining ecosystems worldwide (Tickner et al., 2020; Weise et al., 2020; Onojeghuo et al., 2021). Accelerated climate change and intensified human activities have profoundly disrupted the global hydrological cycle, causing substantial spatial and temporal shifts in water distribution. As a result, wetland areas have undergone dramatic contraction, accompanied by a marked decline in their ecological integrity, functional capacity, and the ecosystem services they provide (Zedler and Kercher, 2005; Wang et al., 2012; Dehua Mao et al., 2022; Wang et al., 2023).

Accurate wetland mapping is essential for monitoring wetland dynamics, understanding ecosystem functions, and analyzing responses to climate change and human activities. Remote sensing is widely used for wetland classification (Xing et al., 2021; Hou et al., 2022; Xing et al., 2023); however, due to spectral confusion—i.e., the phenomena of "same object, different spectra" and "different objects, same spectrum"—relying solely on spectral features often fails to distinguish wetland types effectively. Additionally, wetlands represent a gradual transition between terrestrial and aquatic environments. Their structural complexity and variable inundation conditions often lead to misclassification between vegetated and non-vegetated flooded areas (e.g., marshes and mudflats), resulting in high intra-class and low inter-class variability (Henderson and Lewis, 2008; Dronova, 2015). Furthermore, wetlands are highly dynamic ecosystems and can exhibit abrupt changes in response to water level fluctuations and vegetation growth (Anonymous, 2020; Jamali et al., 2023). At large scales, satellite data often suffer from limited coverage, and classification results are affected by the quality of training samples and algorithms, which hinders both efficiency and accuracy (Hu et al., 2017).

Since 2000, several global and national-scale land cover datasets have been developed (Loveland et al., 2000; Bartholomé and Belward, 2005; Gong et al., 2013), contributing significantly to land cover monitoring worldwide. However, most of these datasets provide only coarse wetland layers and lack detailed spatial information. Recently, NASA developed the Harmonized Landsat–Sentinel (HLS) dataset, which merges Landsat-8 and Sentinel-2 multispectral observations to produce 30 m resolution, 2–3-day revisit global surface reflectance data (Claverie et al., 2018), offering valuable temporal coverage for wetland-related applications. Similarly, The CAS Wetlands dataset, developed by the Northeast Institute of Geography and Agroecology, Chinese Academy of Sciences, offers national-scale wetland distribution data based on medium-resolution satellite imagery(10-30m) (Jia et al., 2014, 2018; Mao et al., 2018a, 2018b; Jia et al., 2019; Mao et al., 2019; Ren et al., 2019; Mao et al., 2020), Although both datasets are useful for large-area monitoring, their 30 m spatial resolution is insufficient to delineate small, fragmented, or morphologically complex wetland types such as mangroves, salt marshes, and irrigation ditches. These limitations often lead to boundary ambiguities and class confusion in heterogeneous coastal landscapes.

Hainan Province, located in southern China, is one of the country's most important tropical island wetland regions. It hosts a wide array of wetland types—including mangrove forests, lagoons, estuaries, sandy coasts, and aquaculture ponds—which provide crucial ecosystem services such as biodiversity conservation, carbon storage, coastal protection, and climate regulation. In recent years, wetland conservation in Hainan has received increasing policy attention through initiatives such as the Hainan Ecological Protection Red Line Delineation Plan and the Hainan Wetland Protection Regulations. The province is also part of China's "Ecological Civilization Pilot Zone" and has implemented key projects such as the Mangrove Protection and Restoration Special Action and the Blue Carbon Pilot, further highlighting the strategic role of tropical wetlands in achieving national carbon neutrality goals. Despite this, current wetland research and mapping in Hainan still rely heavily on medium-resolution imagery, which is insufficient for capturing small, fragmented, and seasonally dynamic wetlands such as mangroves, intertidal salt marshes, and aquaculture facilities. To address this gap, the present study employs multi-source high-resolution satellite imagery, combined with expert-guided visual interpretation and field-based Real-Time Kinematic(RTK) validation, to develop a fine-scale wetland mapping methodology under sub-meter spatial resolution.

Beyond the specific context of Hainan Island, the methodology developed in this study—integrating dual-temporal sub-meter optical satellite imagery (WorldView-2/3, Gaofen-1, Gaofen-2), expert-guided object-based visual interpretation, and RTK-based field validation—offers broad applicability to other coastal and island regions worldwide. This is especially relevant in tropical and subtropical zones, where persistent cloud cover, complex landscape heterogeneity, and dynamic tidal regimes present substantial challenges to conventional wetland mapping approaches. The dual-season fusion effectively captures seasonal hydrological variability, while the sub-meter resolution ensures precise delineation of wetland patches as small as 0.0004 km². Such methods are particularly valuable for detecting fragmented, narrow, or transient wetland features that are often overlooked or misclassified in medium-resolution datasets. By combining very high-resolution (VHR) imagery with human-in-the-loop interpretation, this study demonstrates a significant improvement in both the accuracy and thematic granularity of wetland classification, especially for ecologically critical types such as mangroves, intertidal marshes, and aquaculture ponds. From a remote sensing perspective, this work advances the integration of multi-source imagery and fine-scale classification systems, providing a practical and transferable framework for high-precision habitat monitoring, biodiversity conservation, and ecosystem service assessment, including blue carbon accounting. To our knowledge, this is the first study to produce a full-province wetland map of Hainan Island using multi-source sub-meter satellite imagery. Compared with widely used medium-resolution products such as Landsat, Sentinel-2, or Harmonized Landsat-

FIGURE 1
Study area.
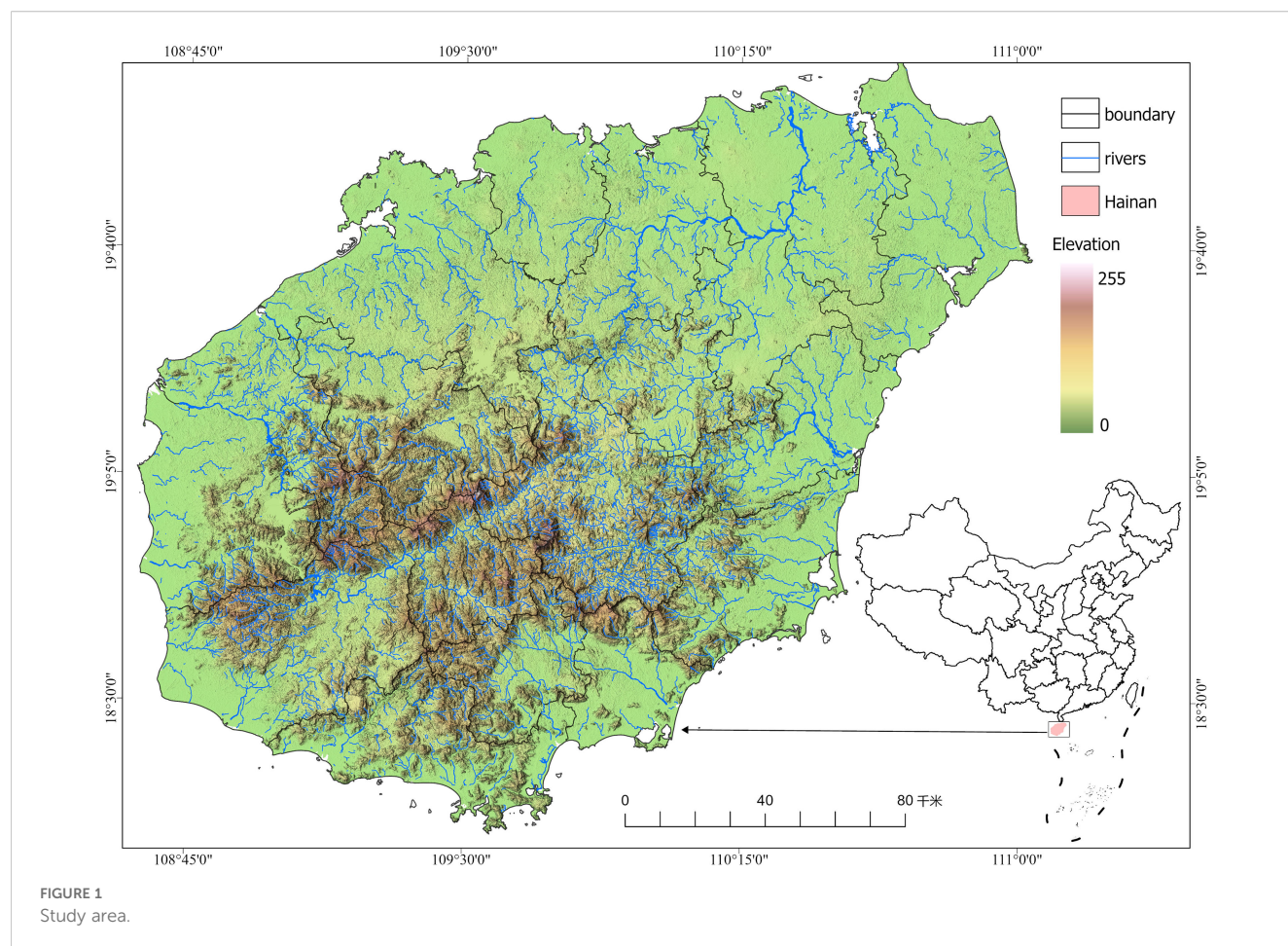
Sentinel (HLS), our approach exhibits clear advantages in identifying fragmented and seasonally dynamic wetland patches that are difficult to detect at coarser scales. The resulting dataset enhances thematic detail and ecological representativeness, providing robust support for ecological management, spatial planning, and climate mitigation efforts in tropical island environments.

2 Materials and methods

2.1 Study area

Hainan Island is located between 18.21°N and 20.21°N latitude and 108.67°E and 111.27°E longitude (Figure 1), situated in the outer tropical zone of the northern South China Sea. It is the largest tropical island in China, with a total land area of approximately 35,400 km². The island is bounded by the Qiongzhou Strait to the north and the South China Sea to the south. Hainan experiences a typical East Asian monsoon climate, with a distinct dry season from November to April and a rainy season from May to October. Annual precipitation ranges from 1,500 to 2,000 mm, of which 35–70% is influenced by typhoons. The average annual temperature is around 24.0°C.Topographically, the island is characterized by mountainous terrain in the central region, gradually sloping toward the surrounding coastal plains. This landscape supports a dense and well-developed river network, with numerous rivers and estuaries connecting the mountainous interior to the sea. The coastal wetlands of Hainan Island are diverse and widely distributed, encompassing various types of ecosystems that are shaped by both natural and anthropogenic processes.

2.2 Satellite image collection and pre-processing

In this study, high-resolution remote sensing images obtained from the 2019 Hainan Provincial Basic Mapping Project were used as the main data source, and the presentability and low cloud coverage of the data were prioritized during the image selection process, so as to ensure the geometric accuracy and radiometric consistency of the orthophotographs, and to satisfy the requirements for interpreting the wetland patches on the sub-meter scale. The image dataset covers the whole year of 2019, with 827 views (Table 1), including 439 views in the first half of the year (January to July) and 388 views in the second half of the year (August to December). At the beginning of the project, images from the WorldView series satellites (WorldView-2 and WorldView-3) provided by Maxar Corporation of the U.S. were used as the main data source because of their excellent spatial resolution (panchromatic 0.5 m, multispectral 2 m) and rich spectral bands,

TABLE 1 Imaging data collected in this study.

Phase	Data type	Time	Number (views)	Full color resolution	Multi-spectral resolution
First half	GeoEye-1	February-July 2019	67	0.5m	2m
	WorldView-2	January-July 2019	187	0.5m	2m
	WorldView-3	February-June 2019	44	0.5m	2m
	GJ1	February-July 2019	131	0.5m	2m
	PL0	February-July 2019	2	0.7m	2.8m
	GF2	April-July 2019	4	0.8m	3.2m
	SPOT6	January-May 2019	4	1.5m	6m
Last-half year	GeoEye-1	September-December 2019	60	0.5m	2m
	WorldView-2	September-December 2019	96	0.5m	2m
	WorldView-3	September-December 2019	12	0.5m	2m
	GJ1	September-December 2019	166	0.5m	2m
	PL1	August-December 2019	40	0.7m	2.8m
	GF2	November 2019	5	0.8m	3.2m
	SPOT6	August-December 2019	9	1.5m	6m

which can effectively identify complex wetland types. However, due to the tropical monsoon climate of Hainan Island, the year-round cloudiness is high, resulting in insufficient data coverage in some areas. To solve this problem, the research team established a flexible data replacement mechanism by incorporating other multi-source high-resolution images (GeoEye-1, GaoJing-1, GF-2, PlanetScope-0/1, SPOT-6) based on actual acquisition conditions, on the premise that the data were acquired around the same time and have consistent or similar spatial resolutions.

These data sources take into account spatial resolution, spectral features, and accessibility, effectively ensuring seamless coverage of the whole island and consistency in image quality. In addition, images from the first half of the year (period characterized by abundant water) and the second half of the year (dry period) were selected for joint mapping, with the intention of utilizing seasonal water level differences to reveal the dynamic characteristics of wetlands. For example, some seasonal wetlands, floodplains, or intertidal zones exhibit obvious inundation and exposure changes in different seasons, which are difficult to accurately identify by relying on single-phase images alone. The joint application of dual-time-phase images can effectively improve the recognition accuracy of wetland boundaries, reduce the omission of patches, enhance the responsiveness of classification results to seasonal hydrological fluctuations, and enhance the timeliness and scientificity of the mapping results.

These multi-source datasets balanced spatial resolution, spectral characteristics, and data availability, ensuring seamless coverage of the entire island and uniform image quality. Furthermore, dual-temporal imagery from both the wet season (first half of the year) and dry season (second half) was integrated to capture seasonal hydrological dynamics. This approach enabled the detection of temporal variations in water levels, which is critical for identifying features such as seasonal wetlands, floodplains, and intertidal zones

that exhibit pronounced inundation and exposure shifts. The integration of dual-phase imagery significantly enhanced the accuracy of wetland boundary delineation, reduced omission of small patches, and improved the responsiveness of classification results to seasonal hydrological fluctuations, thereby increasing both the timeliness and scientific robustness of the final wetland map.

Reference data from the Hainan International Tourism Island Digital Geospatial Framework Construction Project and the 2019 Hainan Satellite Imagery Field Points were collected. The 2000 National Geodetic Coordinate System and the 1985 National Elevation Datum were used to georeference and validate the orthophoto outputs (Figure 2).

Image control points were manually placed, with field-measured control points serving as the fundamental georeferencing data. Panchromatic image correction, multispectral image alignment, and image fusion were performed using PCIGeomatics GXL 2018 through regional block adjustment. Subsequently, GeowayCIPS 2.0 was used for band reorganization, resolution downscaling, and radiometric balancing (including brightness and color correction), resulting in the final orthorectified imagery for the entire study area (Figure 3).

2.3 Wetland classification system

The Ramsar Convention defines wetlands as areas of marsh, fen, peatland, or water—whether natural or artificial, permanent or temporary—where water may be static or flowing, fresh, brackish, or saline. It also includes marine areas with a depth not exceeding 6 meters at low tide (Gong et al., 2010; Mao et al., 2020). This definition is widely adopted due to its comprehensive coverage of global wetland characteristics. In this study, we adopt the Ramsar
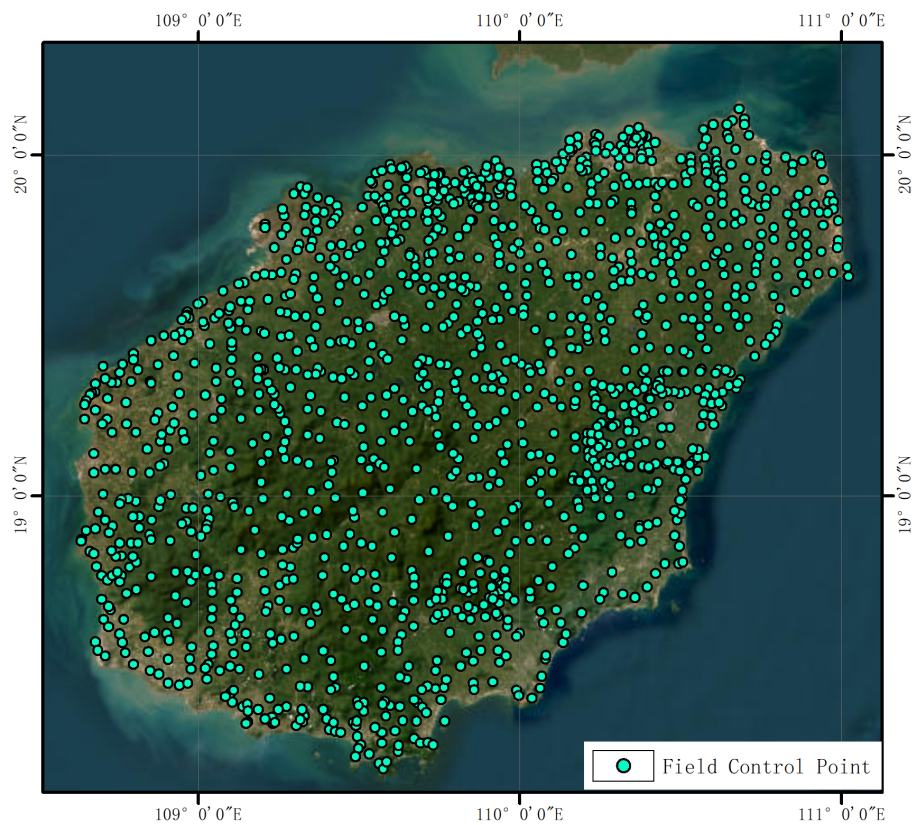
FIGURE 2
Hainan island image control point.

definition and further refine it to reflect the specific ecological features of tropical island wetlands. Accordingly, wetlands on Hainan Island are classified into 3 major categories and 17 subcategories (Table 2). This classification system not only aligns with the Ramsar Convention, facilitating international recognition and comparison, but also highlights the unique characteristics of Hainan's wetland ecosystems. Although coral reefs and seagrass beds are ecologically important and relatively typical wetland types on Hainan Island, their spatial extent cannot be accurately delineated through manual visual interpretation alone. As a result, they were not classified as independent categories in this study, but were instead subsumed under broader categories such as shallow marine waters or sandy coasts.

Although paddy fields and mossy swamps are recognized as important wetland types in many international and national classification systems, they were deliberately excluded from this study due to ecological relevance and policy considerations. Paddy fields, while exhibiting certain hydrological characteristics of wetlands, are designated as permanent basic farmland under China's land use policy and are legally categorized as agricultural land. Including them in the wetland inventory could blur the distinction between natural and anthropogenic land uses, potentially leading to conflicts in interpretation and undermining the ecological clarity of the dataset. Mossy swamps, on the other hand, are typically found in alpine or subalpine regions and are ecologically irrelevant to the tropical island environment of Hainan.

Historical records and field surveys indicate that such wetland types do not occur within the study area. Although the exclusion of these categories may theoretically limit the typological completeness of the dataset, their absence has negligible impact on the dataset's comprehensiveness and ecological representativeness within the context of Hainan Island. This study prioritizes the delineation of naturally occurring, ecologically meaningful wetland types characteristic of tropical island systems, and the resulting dataset offers high applicability for resource management, biodiversity conservation, and spatial planning in similar environments.

Dual-temporal sub-meter resolution visible imagery (RGB) from the first and second halves of 2019 was employed to accurately map various wetland types through expert-guided visual interpretation. To ensure consistency and high accuracy in interpretation, all interpreters received standardized training, including for recognizing wetland types, using interpretation indicators, correcting common errors, and cognitive matching between field observations and remote sensing imagery. A unified set of interpretation markers was established, and interpreters were required to achieve an accuracy rate exceeding 90%. Wetland extraction was performed using the ArcMap 10.6 platform, with an interpretation scale of 1:1000. Due to the high spatial resolution, wetland patches larger than 0.0004 km² were manually delineated. Based on initial classifications, wetland categories were further refined by incorporating high-resolution image features, geospatial context, seasonal variation, and dynamic characteristics.
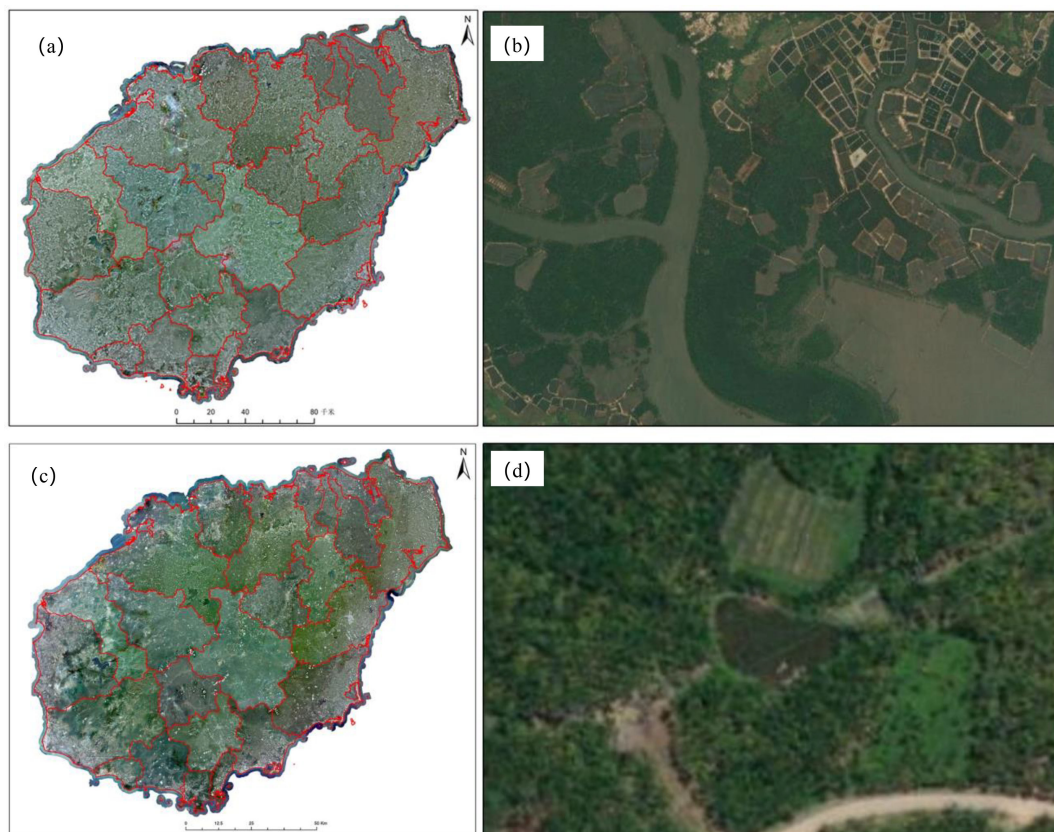
FIGURE 3
2019 synthetic image results: **(a)** first half of the year synthetic image results, **(b)** second half of the year synthetic image results **(c)** clear boundaries of complex wetlands such as mangroves, mudflats, tidal flats, farms, abandoned farms, etc. **(d)** clear boundaries of the 500m² reservoir ponds.

To enhance the accuracy of wetland boundaries, water levels from the two time phases were compared to distinguish areas subject to seasonal inundation or exposure, thereby reducing the omission of features such as reservoir ponds and aquaculture ponds due to temporary drainage (Figure 4). For shallow marine waters, military electronic nautical charts were used to identify the 0 m isobath as the low tide line, while the 5 m and 10 m isobaths were interpolated using Kriging to derive the 6 m depth contour. For estuarine wetlands, the tidal boundary at the river mouth (i.e., zero tidal range zone) was corrected based on field measurements, while upstream boundaries were adjusted using salinity gradients (Figure 5). To ensure data authenticity and spatial precision, estuarine surveys were conducted at high tide using a salinometer to identify the salt–freshwater interface at 1 g/L salinity. These measurements were corroborated with field observations of plant and animal indicators to comprehensively determine tidal boundaries.

2.4 Accuracy validation

Between May and October 2020, the research team conducted a detailed field validation survey across the study area. Stratified random sampling was employed to ensure representative coverage of all wetland types. The number of validation samples for each
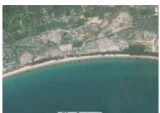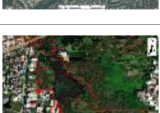
wetland category was determined according to its proportional patch area, ensuring an even spatial distribution. In total, 1,008 validation samples were selected, encompassing all wetland types identified in the classification (Figure 6).

Field validation involved both type verification and boundary correction of the selected samples (Figure 7). High-precision Real-Time Kinematic (RTK) GPS equipment (accuracy within ±0.5 m) was used to record the geographic coordinates of each patch, accompanied by on-site photographic documentation. All fieldwork was carried out in strict compliance with technical protocols. Each wetland patch included no fewer than two survey points or transects. In cases where boundary uncertainty was present, linear survey routes of at least 100 meters in length were established, with wetland boundaries precisely recorded using RTK for subsequent correction. A total of 1,952 point-based validation records and 139 linear transects were collected during the field campaign. To ensure data accuracy and consistency, a two-person cross-checking method was implemented throughout the survey process.

2.5 Accuracy assessment

To assess the accuracy of the wetland classification results, this study employed a confusion matrix constructed from RTK-GNSS-

TABLE 2 Wetland classification system for remote sensing.

Category I	Category II	Description	Image example
Coastal wetland	Shallow marine water	Marine water bodies between the coastline and the 6-meter depth contour include bays and straits.	
	Bedrock coast	The bottom substrate is more than 75% rock and gravel, including rocky coastal islands, and sea rock cliffs.	
	Sandy coast	Sparse beaches consisting of sandy or sandy gravel with <30% vegetation cover.	
	Mudflat	Silt beach with <30% vegetation cover composed of silt.	
	Coastal marsh	Intertidal beaches with vegetation cover ≥ 30% between above the low tide line (not included) and below the high tide line (including the high tide line).	
	Mangrove	An intertidal marsh dominated by mangrove plants.	
	Estuarine water	The permanent body of water between the tidal zone boundary (zero tidal range) in the near mouth section and the edge of the freshwater tongue front in the waterfront section outside the mouth.	
	Lagoon	A lake located in a waterfront area with one or more narrow waterways connected to the sea.	
Inland wetland	River	Streams with perennial stream runoff, including only the bed portion of the stream.	
	Floodplain	It consists of flooded riverbanks, river heartlands, river valleys, seasonally flooded grasslands, and inland deltas that remain perennially or seasonally inundated with water during the high water season.	
	Lake	Natural polygonal stagnant water bodies in inland areas	
	Inland marsh	Freshwater marshes with dominant communities of aquatic and marshy herbaceous plants.	

(Continued)

TABLE 2 Continued

Category I	Category II	Description	Image example
	Inland swamp	Freshwater marshes with a dominant community of scrub and tree plants.	
Artificial wetland	Reservoir/pond	A water storage area constructed for the primary purposes of water storage, power generation, agricultural irrigation, urban landscaping, and rural living.	
	Canal/channel	Artificial fluvial wetlands constructed for water conveyance or transportation, including ditches and canals where irrigation is the primary purpose.	
	Aquaculture pond	Artificial wetlands constructed for the primary purpose of aquaculture.	
	Salt pan	Salt tanning sites or salt ponds, including salt ponds and brine springs, constructed for the purpose of obtaining salt resources.	

based field validation points. Standard classification accuracy metrics were calculated, including Overall Accuracy (OA), User's Accuracy (UA), Producer's Accuracy (PA), F1-score, and the Kappa coefficient (κ). The confusion matrix was generated using an independent set of validation samples that comprehensively covered the major wetland types, ensuring the representativeness and objectivity of the evaluation. In addition to the overall metrics, class-specific UA (Precision), PA (Recall), and F1-score were calculated to assess the recognition accuracy of each wetland type and to better characterize misclassification patterns. Notably, UA is closely associated with Type I error (false positives), while PA corresponds to Type II error (false negatives), making them valuable for identifying the direction and potential risks of misclassification. These indicators provide critical insights into the classification uncertainties, especially for spectrally similar or spatially adjacent wetland types (e.g., mangroves and salt marshes). Although formal statistical significance tests (e.g., McNemar's test or Z-test) were not conducted to compare classification schemes, the high OA (96.13%) and κ value (0.95), along with favorable class-level F1-scores, indicate that the classification results exhibit strong consistency with the field data and effectively represent the spatial distribution and typological diversity of wetlands across Hainan Island.

3 Results

3.1 Mapping accuracy of wetland maps

Based on 1,008 field validation samples, the classification accuracy of the wetland map was quantitatively assessed and summarized in

Table 3. The overall classification accuracy reached 96.13%, with a Kappa coefficient of 0.95, indicating strong agreement between the classification results and ground-truth data. Specifically, 12 out of 17 categories achieved PA above 95%, with five types (shallow marine water, estuarine water, lagoon, inland marsh, and inland swamp) reaching 100% PA, corresponding to 0 Type II errors. The lowest PA values were found in coastal marsh (85.71%) and mudflat (86.67%), with Type II errors of 2 and 2 respectively, primarily due to confusion with adjacent classes such as mangroves and sandy coasts. In terms of UA, 13 categories exceeded 90%, and several (e.g., shallow marine water, river, and reservoir/pond) achieved over 96%, indicating low Type I error rates. The lake class had the lowest UA (87.5%), due to 1 Type I error, where a reservoir pond was incorrectly included in the lake category. The highest Type I error counts were observed in aquaculture pond (10 cases) and sandy coast (4 cases), suggesting minor commission errors, yet these categories still maintained UA levels above 89%. In addition, the F1-score was calculated for each category to assess the harmonic balance between UA and PA. The average F1-score across all classes was 96.14%. Most wetland types achieved F1-scores above 95%, with the exception of coastal marsh (88.89%), sandy coast (89.19%), and mudflat (89.66%), reflecting slight but acceptable classification ambiguity in spectrally overlapping zones. Notably, 12 of 17 classes had F1-scores ≥ 95%, demonstrating strong robustness and reliability of the classification framework.

3.2 Area and distribution of Hainan's wetlands

The wetland area statistics for Hainan Island in 2019 are presented in Table 4. Wetlands with a patch size ≥0.0004 km²

FIGURE 4
Comparison of the first and second half of the wetland images: **(a, b)** water level changes in the reservoir pond in the first and second half of the year; **(c, d)** seasonal discharge of water from the reservoir pond.

totaled 3842.84 km². As shown in Figure 8, wetlands are widely distributed across the island, primarily concentrated in the peripheral alluvial plains and coastal waters. A smaller number of reservoir ponds, aquaculture ponds, and rivers are located in the central mountainous region. Spatially, wetlands exhibit distinct distribution patterns: inland areas have fewer wetlands than coastal areas; eastern regions have more than western ones; and the north contains more than the south. Overall, wetland patches are numerous and spatially fragmented, reflecting high spatial heterogeneity.

Coastal wetlands account for 2075.08 km², representing 54% of the total wetland area. Among these, shallow marine waters are the dominant type (1462.31 km², 70.47% of coastal wetlands; 38.05% of all wetlands), providing essential habitats for marine organisms such as coral reefs and seagrass beds. As a popular tourist destination, Hainan Island is surrounded by abundant beach resources. Among the coastal wetland types, sandy coast ranks second in area after shallow marine waters, covering 354.95 km² and accounting for 9.24% of the total wetland area., while lagoons, a unique coastal wetland type, are primarily found along the eastern shoreline, with a total area of 92.6 km². Rocky coasts are mainly distributed in the northeast and southeast, occupying 54.72 km²,

and estuarine waters cover 54.03 km² and are concentrated at the outlets of Hainan's three major river basins: the Nandu, Wanquan, and Changhua rivers. Hainan is the most mangrove-rich province in China, hosting 44 species from 21 families and 28 genera. Mangrove forests are primarily located in intertidal zones such as lagoons, estuaries, and harbors, covering an area of 53.12 km². Mudflats are found in low-energy coastal environments and span 3.27 km². The smallest coastal wetland type is coastal marsh, with an area of just 0.08 km², dominated by the exotic species Miscanthus intermedia.

Artificial wetlands total 1,374.52 km², accounting for 35.77% of the total wetland area, and are predominantly distributed across the island's plains. The largest category is reservoir ponds, covering 916.41 km² (66.67% of artificial wetlands; 23.85% of total wetlands), making them the second-largest wetland type after shallow marine waters. Aquaculture ponds, primarily located along the coast, total 321.44 km² (23.39% of artificial wetlands). The remaining categories—canals/influent rivers and salt pans—cover 103.67 km² and 33.00 km², respectively.

Inland wetlands are less prevalent, covering 393.24 km² (10.23% of the total). Rivers dominate this category, accounting for 339.84 km² (86.42% of inland wetlands; 8.84% of total wetlands), mostly

FIGURE 5
Field validation of wetlands in estuarine waters: **(a)** field salinity measurements; **(b, c)** marine organisms (oysters, mangrove seedlings) judging salinity and lightness demarcation points.
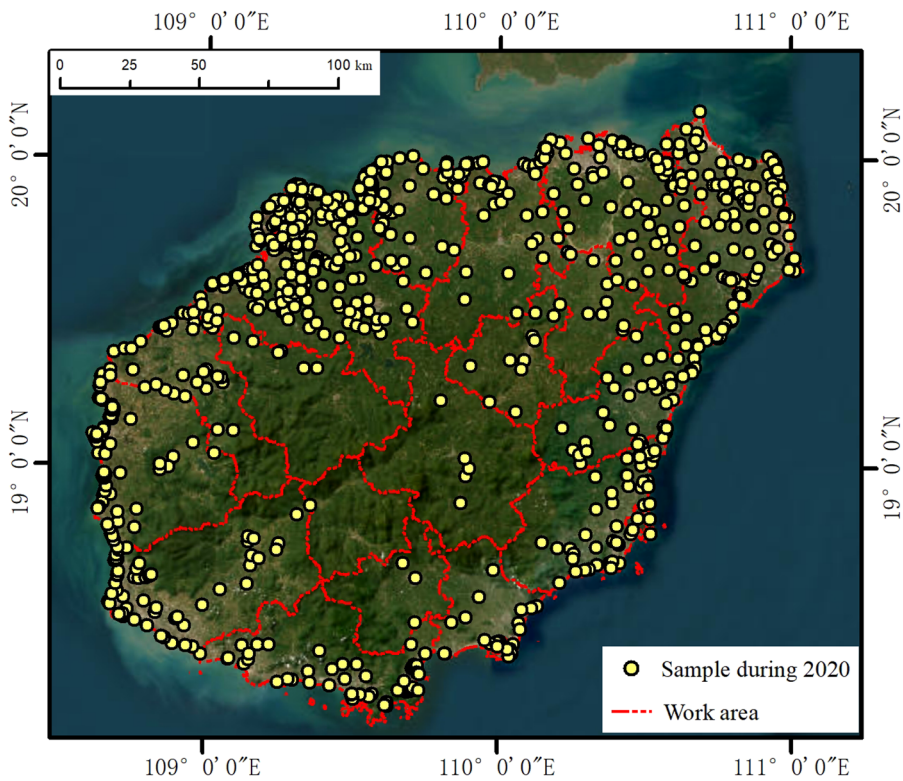
FIGURE 6
Work area field sample locations.
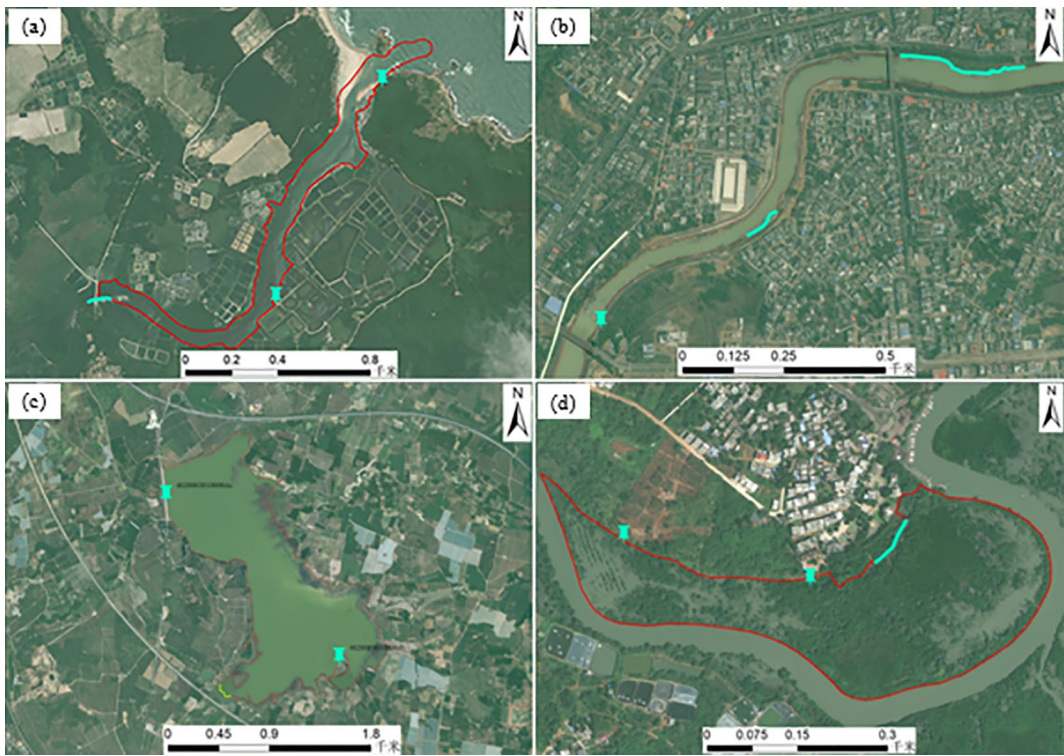
FIGURE 7
Wetland patch field validation routes and points: **(a)** estuarine waters patch field validation points and lines, **(b)** riverine patch field validation points and lines, **(c)** reservoir pond patch field validation points and lines, **(d)** mangrove patch field validation points and lines.

TABLE 3 Classification accuracy.

Category I	Category II	Sample number	PA	UA	Type I error	Type II error	F1-score
Coastal wetland	Shallow marine water	10	100.00%	100.00%	0	0	100.00%
	Bedrock coast	31	93.33%	90.32%	3	2	91.80%
	Sandy coast	37	89.19%	89.19%	4	4	89.19%
	Mudflat	14	86.67%	92.86%	1	2	89.66%
	Coastal marsh	13	85.71%	92.31%	1	2	88.89%
	Mangrove	98	98.97%	97.96%	2	1	98.46%
	Estuarine water	40	100.00%	97.50%	1	0	98.73%
	Lagoon	17	100.00%	94.12%	1	0	96.97%
Inland wetland	River	140	97.89%	99.29%	1	3	98.58%
	Floodplain	24	95.83%	95.83%	1	1	95.83%
	Lake	8	100.00%	87.50%	1	0	93.33%
	Inland marsh	11	100.00%	90.91%	1	0	95.24%
	Inland swamp	22	100.00%	95.45%	1	0	97.67%
Artificial wetland	Reservoir/pond	251	94.53%	96.41%	9	14	95.46%
	Canal/channel	26	96.15%	96.15%	1	1	96.15%
	Aquaculture pond	253	96.43%	96.05%	10	9	96.24%
	Salt pan	13	100.00%	92.31%	1	0	96.00%
Summary		1008	Overall=96.13%	Kappa=0.95	39	39	96.14%

TABLE 4 Wetland area statistics for Hainan Island.

Category I	Area (km²)	Percentage (%)	Category II	Area (km²)	Percentage (%)
Coastal wetland	1884.89	51.60	Shallow marine water	1462.31	38.05
			Bedrock coast	54.72	1.42
			Sandy coast	354.95	9.24
			Mudflat	3.27	0.09
			Coastal marsh	0.08	0.00
			Mangrove	53.12	1.38
			Estuarine water	54.03	1.41
			Lagoon	92.60	2.41
Inland wetland	393.24	10.77	River	339.84	8.84
			Floodplain	51.05	1.33
			Lake	1.66	0.04
			Inland marsh	0.26	0.01
			Inland swamp	0.43	0.01
Artificial wetland	1374.54	37.63	Reservoir/pond	916.41	23.85
			Canal/channel	103.67	2.70
			Aquaculture pond	321.44	8.36
			Salt pan	33.00	0.86
Summary(km²)			3842.84		

FIGURE 8
Distribution of wetland resources on Hainan Island.
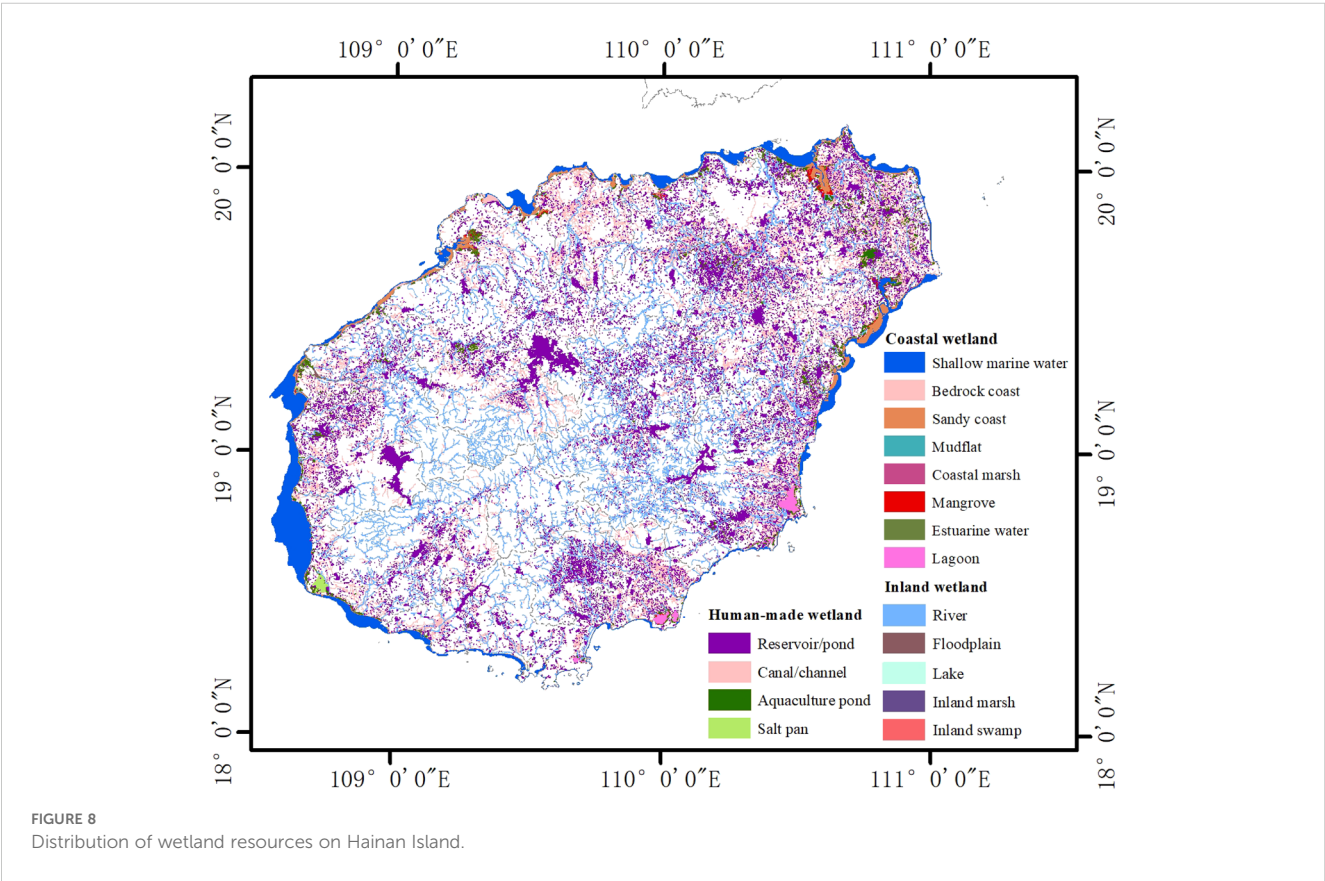
distributed within the island's three major watersheds. Floodplains, associated with these river systems, occupy 51.05 km² (12.98% of inland wetlands) and are primarily found along river valleys in coastal areas. Lakes are rare due to anthropogenic alterations, with a combined area of only 1.66 km². The least represented inland wetland types are inland marshes (0.26 km²) and inland swamps (0.43 km²).

3.3 Inter-comparison with existing datasets

The Second National Wetland Inventory (SNWI), conducted between 2009 and 2013, surveyed lakes, marshes, coastal wetlands, and artificial wetlands with an area of ≥0.08 km², along with riverine wetlands at least 10 meters wide and 5 kilometers long, and other ecologically significant wetland types. The SNWI adopted a relatively fine-grained classification scheme, dividing wetlands into 5 major categories and 34 subcategories, which encompassed all wetland types identified in the present study. According to the SNWI data, the total wetland area in Hainan Province was reported as 3,142.18 km².In contrast, this study identified a total wetland area of 3842.84 km², representing a difference of 700.66 km². The primary reason for this discrepancy is the higher spatial resolution and finer classification used in the present study, which allowed for the inclusion of numerous small wetland patches (<0.08 km²) that were previously unaccounted for.

To enable a fair and intuitive comparison between the two datasets, we recalculated the wetland statistics in this study using only patches ≥0.08 km². This allowed us to assess trends in wetland resources on Hainan Island over the past decade.

As shown in Table 5, the overall wetland area on Hainan Island has remained relatively stable over the past decade, increasing from 3,142.18 km² (as recorded in the SNWI) to 3,335.98 km² in the present survey—a net gain of 193.80 km², representing a 6.17% increase. Among the three major wetland categories, both artificial wetlands and coastal wetlands exhibited area increases of 131.53 km² (+16.86%) and 116.48 km² (+5.95%), respectively, while inland wetlands declined by 54.21 km² (−13.43%). Within the artificial wetlands, the most notable change occurred in canals and transmission rivers, which expanded from 8.41 km² to 17.45 km²—an increase of 9.04 km² or 107.56%. This was followed by aquaculture ponds, which increased by 103.40 km², from 155.62 km² to 259.02 km² (+66.44%). Reservoir ponds also experienced moderate growth, rising from 567.32 km² to 602.32 km² (+35.00 km², or +6.17%). The only artificial wetland type to decrease in area was salt flats, which declined by 15.85 km², from 48.63 km² to 32.78 km² (−32.59%). Among coastal wetland subcategories, the greatest increase was observed in sandy and gravel beaches, which expanded by 90.89 km² (from 264.06 km² to 354.95 km², +34.42%), followed by rocky coasts (+11.22 km², +25.76%) and mangrove forests (+5.16 km², +12.17%). Intertidal salt marshes remained unchanged at 0 km². Some coastal wetland types exhibited area losses, such as estuarine waters, which declined by 15.66 km² (−22.47%), and pale muddy beaches, which decreased by 6.65 km² (−67.04%). Although shallow

TABLE 5 Comparison of wetland data over the last 10 years on Hainan Island (≥0.08km²).

Category I	Data from this study (km²)	SNWI (km²)	Category II	Data from this study (km²)	SNWI (km²)
Coastal wetland	2075.06	1958.58	Shallow marine water	1462.31	1446.95
			Bedrock coast	54.77	43.55
			Sandy coast	354.95	264.06
			Mudflat	3.27	9.93
			Coastal marsh	0.00	0.00
			Mangrove	53.12	47.36
			Estuarine water	54.03	69.69
			Lagoon	92.60	77.04
Inland wetland	349.35	403.56	River	319.60	351.09
			Floodplain	27.90	46.46
			Lake	1.52	5.57
			Inland marsh	0.20	0.44
			Inland swamp	0.12	0.00
Artificial wetland	911.57	780.04	Reservoir/pond	602.32	567.38
			Canal/channel	17.45	8.4063
			Aquaculture pond	259.02	155.6214
			Salt pan	32.78	48.6304
Summary (km²)				3335.9	3142.18

marine waters emain the most extensive wetland type in Hainan, they also recorded the largest absolute decline in area, decreasing from 1,462.31 km² to 1,446.95 km² (−15.36 km², −1.05%). For inland wetlands, the most significant reductions were observed in floodplain wetlands (−18.56 km², −39.14%) and rivers (−31.48 km², −8.97%). The area of lakes decreased markedly from 5.57 km² to 1.52 km² (−4.05 km², −72.71%), while inland marshes showed a slight increase of 0.12 km².

3.4 Geospatial pattern of wetlands in Hainan

The overall spatial distribution of wetlands on Hainan Island is highly uneven, exhibiting a characteristic pattern of "fewer in the center, more around the periphery." Inland areas, particularly the mountainous central region, are dominated by riverine systems with relatively small wetland areas. In contrast, the coastal zones and surrounding lowlands host extensive coastal wetlands and a large number of artificial wetlands, including shallow marine waters, reservoir ponds, and aquaculture ponds, which constitute the largest proportions of the total wetland area. In terms of patch number, there is a dense network of linear wetlands such as rivers and canals, as well as numerous small-sized patches of reservoir ponds and aquaculture ponds. Coastal wetlands are distributed continuously along the island's perimeter. The west coast, with its gentler slope compared to the east, contains a broader -6 m to low tide zone, resulting in a larger area of shallow marine waters than on the east coast. The distribution of mangrove vegetation shows a clear "more in the east, less in the west" pattern. The northeastern coast hosts the most extensive and concentrated mangrove forests, particularly in Dongzhai Harbor (Meilan District, Haikou City) and Qinglan Harbor (Wenchang City). In contrast, mangrove forests are sparsely distributed in the southwest. Although the total mangrove area varies considerably across cities and counties, there is no significant correlation between the number of mangrove patches and their total area—except in Dongzhai Harbor, where both the total area and average patch size are notably large. To further analyze spatial patterns, the island was divided into four quadrants—northeast, southeast, southwest, and northwest—using the geographical center as the origin. The inland wetlands show a "more in the east, less in the west" and "more in the north, less in the south" distribution, with the northeast quadrant containing the largest concentration of inland wetlands. A clear clockwise gradient in wetland abundance is observed. Rivers on the island are strongly influenced by its topography, forming a radial drainage pattern with numerous outflows into the sea. There are 154 independent rivers discharging directly into the ocean. Among them, the Nandu River, Wanquan River, and Changhua River are the three largest, with watershed areas greater than 3,000 km² each. Collectively, these three basins account for approximately 47% of Hainan Island's total land area. The distribution of artificial wetlands also follows a "less in the center, more around the periphery" pattern. As a major marine province in China, Hainan supports a highly developed aquaculture industry. Aquaculture ponds, as a key component of artificial wetlands, are primarily distributed along the coast. In the eastern part of the island, these ponds extend from tablelands to coastal lowlands, including intertidal and offshore zones. Their spatial pattern closely resembles that of natural water bodies such as lakes and rivers. Aquaculture pond density is highest in the northeast and exhibits a clockwise decreasing trend across the island.

In terms of administrative divisions (Table 6), Dongfang City has the largest total wetland area in Hainan Province, reaching 584.00 km². The city hosts a rich diversity of coastal wetland types, including shallow marine water (382.42 km²), Bedrock coast (0.27km²), Sandy coast (18.89km²), Mangrove (17.36 km²), and estuarine water (8.94 km²), which together account for approximately 73.7% of the city's total wetland area. Sand and gravel beaches are widely distributed along the coastline of Dongfang, and a large mangrove forest is located in the Sibi Bay area, which serves as an important wintering habitat for the black-faced spoonbill (Platalea minor), an internationally rare and endangered species. Wenchang City ranks second, with a total wetland area of 558.23 km², including 309.25 km² of coastal wetland. These comprise shallow marine water (196.53 km²), mangrove (11.64 km²), Sandy coast (92.50 km²), and other types. The area supports typical subtidal benthic zones, coral reefs, and mangrove ecosystems, especially around Qinglan Harbor, which is recognized as a representative mangrove wetland in Hainan Province. Danzhou City ranks third in total wetland area, with 429.60 km², of which 234.60 km² are coastal wetlands, including shallow marine water (108.54 km²), Sandy coast (73.83 km²), mangrove (10.31 km²), and Bedrock coast. These account for approximately 54.6% of the city's total wetland area. Danzhou has a winding coastline and a wide variety of wetland types, including shallow seas, mudflats, estuaries, and mangrove forests, forming a mosaic of typical coastal wetland landscapes. Regarding inland wetlands, Haikou City has the largest area, totaling 41.59 km², mainly consisting of rivers (36.24 km²), floodplain (4.83 km²), and a small number of lakes and inland marshes. Ledong County and Qionghai City follow, with inland wetland areas of 40.15 km² and 33.53 km², respectively. In contrast, cities and counties such as Lingao, Lingshui, Baoting, and Tunchang have much smaller inland wetland areas, due to topographic and hydrological limitations. With respect to artificial wetlands, Wenchang City also ranks first, with an artificial wetland area of 238.04 km², accounting for 17.32% of the province's total. It is followed by Danzhou City (173.28 km², 12.61%) and Dongfang City (144.72 km², 10.53%). The dominant artificial wetland types in these regions include reservoir ponds, aquaculture ponds, and Canal/channel, reflecting the intensity of anthropogenic land use. In comparison, six inland administrative regions—Wuzhishan City, Ding'an County, Tunchang County, Baisha County, Baoting County, and Qiongzhong County—have the smallest total wetland areas, each less than 100 km². Among them, Wuzhishan City has the lowest wetland coverage in the province, with only 20.11 km², primarily due to its location in a central mountainous region characterized by high elevation, steep slopes, and limited surface water accumulation, lacking the geomorphological and hydrological conditions necessary for the development of extensive wetlands.

TABLE 6 Area of wetlands in cities and counties on Hainan Island.

No.	City/County	Coastal wetland (km^2)	Inland wetland (km^2)	Artificial wetland (km^2)	Summary (km^2)	Percentage (%)
1	Haikou City	200.93	41.59	124.20	366.71	9.54
2	Sanya City	126.90	15.96	58.28	201.14	5.23
3	Wuzhishan City	0.00	15.39	4.71	20.11	0.52
4	Qionghai City	111.13	33.53	80.93	225.59	5.87
5	Danzhou City	234.60	21.73	173.28	429.60	11.18
6	Wenchang City	309.25	10.93	238.04	558.23	14.53
7	Wanning City	117.76	16.41	93.15	227.32	5.92
8	Dongfang City	412.09	27.19	144.72	584.00	15.20
9	Ding'an County	0.00	13.12	48.89	62.01	1.61
10	Tunchang County	0.00	9.69	31.18	40.87	1.06
11	Chengmai County	73.71	30.74	58.53	162.98	4.24
12	Lingao County	92.03	8.55	40.78	141.36	3.68
13	Baisha County	0.00	23.36	43.56	66.93	1.74
14	Changjiang County	53.24	31.83	31.64	116.72	3.04
15	Ledong County	280.96	40.15	93.77	414.89	10.80
16	Lingshui County	62.49	9.48	37.30	109.27	2.84
17	Baoting County	0.00	10.03	24.11	34.14	0.89
18	Qiongzhong County	0.00	33.54	47.44	80.98	2.11

4 Discussion

4.1 Strengths and reliability of the present data

This study presents several key advantages in high-resolution wetland mapping for Hainan Island:

First, the integration of sub-meter, dual-temporal (wet and dry season) multi-source optical imagery enabled accurate detection of seasonal hydrological variation—for example, the stark contrast between inundated floodplains during the rainy season and exposed bare land in the dry season. This approach effectively mitigates the well-known issues of spectral confusion—namely, "same object, different spectra" and "different objects, same spectrum"—that often hinder medium-resolution, single-phase imagery (Henderson and Lewis, 2008; Dronova, 2015).

Second, the overall classification accuracy achieved was 96.13% ($\kappa = 0.95$), which surpasses existing national-scale wetland products such as CAS_Wetlands (Landsat 8 OLI, 30 m; 95.1% accuracy), GWL_FCS30 (30 m; 89.2% accuracy) (Zhang et al., 2023), and even globally harmonized datasets like Harmonized Landsat-Sentinel (HLS, 30 m), which, although offering improved temporal frequency and radiometric consistency, still lack the spatial resolution required to distinguish fragmented or narrow wetland features. The combination of high-resolution texture features with expert ecological knowledge through human–machine collaborative interpretation significantly enhances the accuracy of classifying complex wetland types such as estuarine waters, floodplains, and ditches. The boundary precision for mangrove forests, intertidal salt marshes, and shallow marine waters was further refined using salinity gradients, biological indicators during high tide, and isobath data from electronic nautical charts (localization error < ± 0.5 m).

Third, 827 high-resolution images with less than 10% cloud cover were selected to ensure seamless, cloud-free coverage across the entire island. This avoids the spatial and temporal discontinuities that often arise from high cloud cover (>30%) in commonly used datasets such as Landsat and Sentinel.

Fourth, this study employed a refined classification framework based on the Ramsar Convention, consisting of 3 major categories and 17 subcategories. Unlike coarser systems such as CAS_Wetlands with 14 classes, GWL_FCS30 with 8 classes, or HLS-based land cover classifications typically offering limited wetland detail due to 30 m resolution, our framework differentiates wetland types by vegetation structure (e.g., mangrove trees vs. halophytes), tidal regime (e.g., high- vs. low-tide zones), and substrate composition (e.g., mud, sand, gravel). This avoids lumping functionally distinct wetlands—such as mangrove forests and intertidal salt marshes—into the same class and enhances both ecological specificity and management relevance. Finally, this classification revealed the rapid expansion of artificial wetlands (e.g., reservoir ponds and aquaculture ponds) in Hainan

since the SNWI, aligning with global trends in coastal development (Murray et al., 2019). It also enabled quantification of the fragmentation characteristics of mangrove patches, many of which have an average area of less than 1 km². This has direct implications for carbon sink estimation and biodiversity habitat assessment based on functional attributes. The high-resolution, functionally oriented data outputs also support more targeted conservation strategies, such as floodplain restoration, mangrove rehabilitation, salt marsh protection, and the regulation of artificial wetlands—thereby significantly enhancing the precision and efficiency of wetland management and restoration decision-making.

4.2 Significance of the present data

Based on dual-phase, sub-meter resolution multi-source imagery and human–computer collaborative interpretation, this study produced fine-scale maps of 17 wetland subcategories across Hainan Island. These maps provide high-quality data support for ecological management efforts, including the delineation of Hainan's ecological protection "red lines" and the implementation of the Ramsar Convention. Compared to the SNWI, which used medium-resolution imagery (19.5 m) and only considered wetland patches ≥0.08 km², our results offer significantly improved spatial precision. Key ecological elements such as mangrove coastlines, intertidal salt marshes, and shallow marine waters were delineated with localization errors of less than ±0.5 m. This enables accurate definition and dynamic monitoring of core and buffer zones within protected areas, thereby supporting fine-scale planning and management under Hainan's ecological zoning framework. For biodiversity conservation, the precise mapping of mangrove forests provides critical input for evaluating ecosystem functions such as carbon sequestration (Mitsch et al., 2013). The refined classification system—comprising 17 wetland subcategories —allows for detailed habitat differentiation, accommodating species with distinct ecological requirements. With sub-meter patch extraction and high-resolution habitat layers, conservation authorities at various administrative levels can implement targeted monitoring and protection measures, enhancing the management effectiveness of national nature reserves and provincial wetland parks. In terms of ecosystem management, the present dataset not only reveals the rapid expansion of artificial wetlands (e.g., reservoir ponds and aquaculture farms) in contrast to the SNWI, but also enables the quantification of human activity intensity through the accurate mapping and classification of wetland types such as salt flats and ditches. This information supports decision-making in aquaculture development, agricultural irrigation planning, and regional water resource allocation. In particular, the spatial heterogeneity analysis of pond systems offers valuable insights for local water management strategies and aligns with the monitoring objectives of Sustainable Development Goal (SDG) 6.6.1 on wetland conservation (Weise et al., 2020). Furthermore, the seamless, cloud-free imagery used in this study greatly reduces the temporal discontinuities common in medium-resolution products due to cloud-masking. This enhances

the real-time reliability of time-series analyses and disaster response applications—for instance, assessing the impacts of typhoon-induced coastal siltation and sand encroachment. Looking ahead, the dataset can be integrated with models such as InVEST and spatial autoregressive frameworks to assess carbon storage, hydrological regulation, and water purification functions. It also provides key parameters for designing carbon-neutral and wetland restoration projects in Hainan. Future research could further incorporate hyperspectral, LiDAR, and SAR data to model vegetation functional groups, soil organic carbon, and methane emissions. Such advancements would provide robust technical support for the long-term dynamic monitoring and adaptive management of tropical wetland ecosystems.

In addition to its relevance for regional planning and management, the fine-scale wetland classification system and high-resolution dataset established in this study possess strong potential for broader application in international contexts. Many tropical and subtropical coastal regions, particularly in Southeast Asia, the Caribbean, and West Africa, face similar challenges in wetland mapping due to persistent cloud cover, fragmented landscapes, and limited field access. The dual-season imagery integration and human–computer collaborative interpretation techniques employed in this research offer a replicable and adaptable workflow for producing ecologically meaningful, spatially detailed wetland inventories under such constraints. Furthermore, by delineating key habitats such as mangroves, salt marshes, and aquaculture ponds with sub-meter accuracy, the dataset aligns with the global priorities of the Ramsar Convention and supports blue carbon assessment, ecosystem restoration planning, and climate-resilient coastal management in line with UN Sustainable Development Goals (e.g., SDG 14.2 and 13.1). Notably, the approach developed in this study also complements and enhances existing satellite-based wetland monitoring frameworks, such as POLWET in Poland (Dabrowska-Zielinska et al., 2016), Global Wetland Watch (UNEP-DHI, 2024), and GlobWetland Africa (Guzinski, 2019). While these programs have significantly advanced wetland monitoring through medium-resolution remote sensing (e.g., Landsat, Sentinel), they often face limitations in capturing fragmented or narrow wetland types in complex coastal settings. By integrating sub-meter imagery, refined classification schemes, and local field validation, our method addresses these resolution gaps and provides a more detailed and transferable mapping solution. This offers valuable synergy for countries aiming to enhance their national wetland inventories and improve compliance with international conservation commitments under the Ramsar Convention and the Sustainable Development Goals.

4.3 Analysis of discrepancies with the SNWI

Through comparative analysis, several key factors were identified as the primary sources of discrepancy between this study and the Second National Wetland Inventory (SNWI). These factors include differences in image resolution, wetland boundary

delineation methods, changes in wetland properties, rapid development of aquaculture, and improved awareness of wetland ecological protection:

4.3.1 Differences in image data accuracy

The SNWI utilizes CBERS-CCD data with a spatial resolution of 19.5 meters, whereas this study employed multi-source composite satellite imagery with a sub-meter resolution of 0.5 meters. Due to the lower resolution of the SNWI data, wetland patch boundaries are often generalized, resulting in the underestimation of certain wetland types such as rivers, lakes, and rocky coasts.

4.3.2 Differences in boundary delineation methods

In the SNWI, coastal wetlands—particularly shallow marine waters—are delineated based on limited-resolution imagery, leading to boundary inaccuracies. In contrast, this study incorporated electronic nautical chart data to refine the low-tide line using 0 m isobaths. Additionally, 5 m and 10 m isobaths were interpolated to generate the 6 m contour line, providing more precise spatial definitions. Moreover, the SNWI merged wetland patches within 100 meters of each other into a single polygon, whereas this study applied a stricter threshold of 30 meters, allowing finer differentiation between adjacent features (Figure 9).

4.3.3 Changes in wetland properties

Land use changes and anthropogenic disturbances have led to significant alterations in wetland characteristics. Some wetlands have been converted to other land uses, degraded, or abandoned due to urban expansion, pollution, or agricultural intensification. For example, several aquaculture ponds have been reforested, salt pans have been repurposed as aquaculture ponds, lakes have been dammed into reservoirs, and some reservoirs have been filled for real estate development (Figure 10).

4.3.4 Rapid development of the aquaculture industry

The increase in artificial wetland area is largely driven by the expansion of aquaculture ponds, reflecting economic policies that promote coastal development (Wang et al., 2012). Since the early 2000s, Hainan Province experienced a surge in aquaculture activities aimed at boosting local economies and alleviating poverty among coastal communities. However, this expansion also led to the degradation and loss of natural coastal wetlands, particularly mangrove forests. It was not until 2018, when Hainan was designated as an Ecological Civilization Pilot Zone, that the expansion trend began to stabilize.

4.3.5 Enhanced awareness and policies for wetland protection

In recent years, national and provincial governments have placed increasing emphasis on ecological conservation. Hainan Province has issued a series of regulations and promoted public education campaigns on wetland protection, improving public awareness and encouraging environmental impact assessments. Scientific research has also advanced wetland restoration techniques and compensation mechanisms. As a result, numerous new nature reserves and wetland parks have been established, contributing to a significant increase in the wetland protection rate. Notably, the declining trend in mangrove forests has been reversed, and the area of mangroves has grown substantially in recent years.

In summary, the discrepancies between our study and the SNWI can be attributed not only to methodological enhancements—such as the use of sub-meter resolution imagery, refined boundary delineation, and stricter patch aggregation criteria—but also to well-documented socio-environmental drivers. Land use transformation, particularly the rapid expansion of coastal aquaculture and urban development, has profoundly altered wetland spatial patterns in recent decades (Liu and Hu, 2019). In addition, China's shift in coastal policy—from reclamation-based development to integrated ecological protection under the "ecological civilization" framework—has substantially
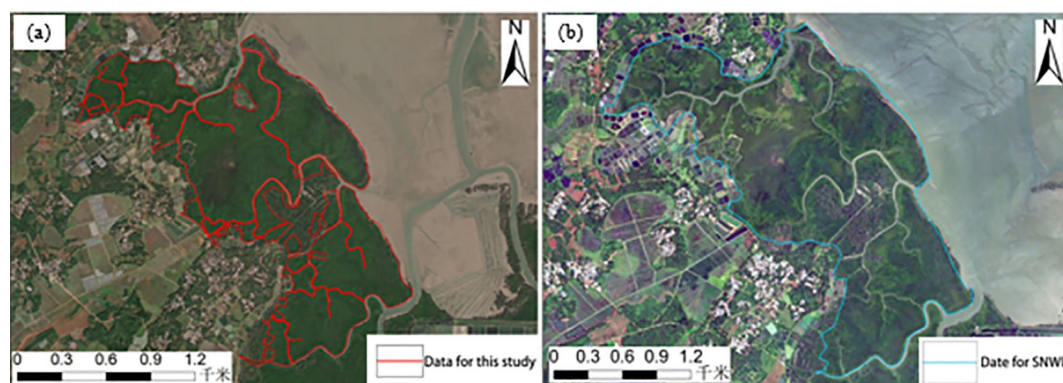

FIGURE 9
Comparison of the boundaries of the present study and the SNWI: **(a)** the present study separates the mangrove forests from the tidal flats, which increases the fragmentation of the patches; **(b)** the SNWI synthesizes the fragmented patches into a whole patch due to the low resolution of the images.
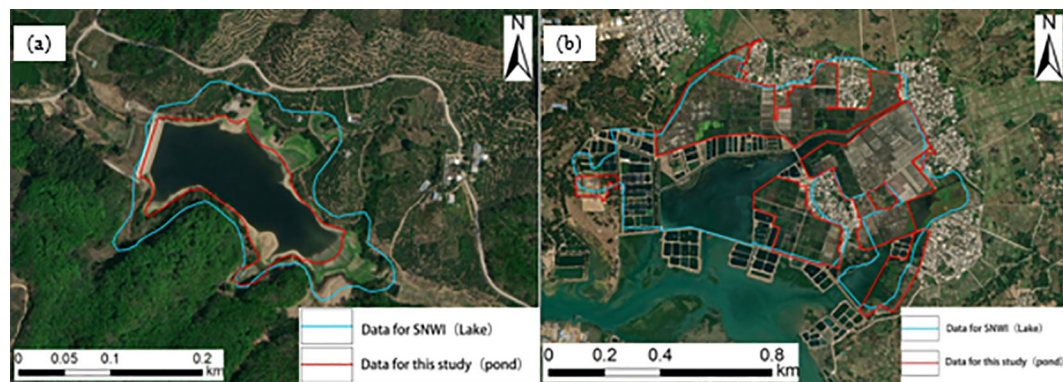
FIGURE 10
Changes in wetland types: **(a)** Lakes changed to reservoir ponds **(b)** Salt pan abandoned and changed to Aquaculture pond.

influenced wetland governance outcomes (Suzhen Yang et al., 2022). Although climate variability, such as sea-level rise and hydrological changes, may exert long-term effects on wetland dynamics (Zhi et al., 2022), its influence on short-term wetland mapping discrepancies is considered secondary. Overall, the observed differences primarily reflect the interplay of methodological improvement, anthropogenic activity, and evolving conservation policies.

4.4 Study Limitations and Future Work

Although the wetland classification framework developed in this study exhibited robust performance—achieving an overall accuracy of 96.13% and a Kappa coefficient of 0.95—several limitations remain that merit further exploration and methodological refinement.

First, persistent cloud cover in tropical island environments such as Hainan significantly constrains the acquisition of cloud-free, high-resolution optical imagery, limiting both the spatial and temporal continuity of remote sensing data. While this study mitigated the issue by integrating dry- and wet-season imagery from 2019, data gaps and temporal mismatches still affected certain regions, potentially compromising classification reliability. To address this challenge, future research should prioritize the integration of cloud-penetrating sensors such as Synthetic Aperture Radar (SAR), alongside optical data from platforms like Sentinel-2, PlanetScope, and WorldView, to enhance the robustness and temporal consistency of wetland monitoring. Previous studies have demonstrated the effectiveness of combining optical and microwave datasets in distinguishing complex wetland habitats under variable atmospheric and hydrological conditions (Hamid et al., 2024).

Second, despite the use of dual-temporal imagery and the inclusion of texture and spatial features, spectral confusion remains a challenge among wetland subtypes with similar reflectance characteristics— particularly mangroves, aquaculture ponds, and tidal flats. Prior research has reported misclassification rates exceeding 30% in such contexts (Mahdianpari et al., 2020). Recent advances in machine learning and deep learning—especially convolutional neural networks (CNNs) (Pouliot et al., 2019) and semantic segmentation models—offer significant potential for addressing this issue. These methods not only

improve classification accuracy but also allow for the quantification of feature importance (e.g., NDVI, SAR backscatter, texture metrics), thereby enhancing the transparency and interpretability of model outputs. Furthermore, they enable the detection of land cover change intensity and the spatial mapping of human interventions across diverse habitats such as wetlands and grasslands.

Third, while the use of expert-guided interpretation improves the accuracy of boundary delineation, it inevitably introduces subjectivity and limits reproducibility. To reduce reliance on manual interpretation, future research should explore scalable, automated classification workflows supported by cloud-based platforms (e.g., Google Earth Engine) and pre-trained models (Bartold et al., 2025). These tools can help reduce labor intensity, improve standardization, and facilitate frequent data updates. In this context, the modular framework developed in this study—based on multi-source image fusion, rule-based object segmentation, and expert input—provides a solid foundation for integration into automated classification pipelines suitable for large-scale applications.

Finally, this study provides a static snapshot of wetland distribution based on 2019 imagery and field validation in 2020. However, the dynamic nature of wetland ecosystems—driven by seasonal hydrology, human activity, and climate variability—necessitates a more temporally responsive approach. To support long-term monitoring and early warning, future research should focus on constructing multi-year time-series datasets for trend analysis, resilience assessment, and uncertainty evaluation. The integration of diverse remote sensing sources, including optical, SAR, LiDAR, and hyperspectral data, with automated, learning-based classification frameworks holds great promise for advancing high-frequency, scalable wetland monitoring and supporting evidence-based ecosystem management.

5 Conclusions

In this study, we developed and applied a wetland mapping framework for Hainan Island that integrates dual-temporal, sub-meter multi-source high-resolution optical imagery, human–machine collaborative interpretation, and on-site RTK validation. This approach enabled the fine-scale classification of 17 wetland subcategories across

the island, resulting in a total mapped wetland area of 3842.84 km² for the year 2019. Of this area, coastal wetlands accounted for 54%, inland wetlands for 10.23%, and artificial wetlands for 35.77%. By leveraging seasonal differences between the wet and dry periods and conducting water level comparisons across image phases, issues such as spectral confusion (e.g., same-spectrum/different-object) and boundary ambiguity were effectively addressed in this study. Combined with high-precision RTK validation, this method achieved an overall classification accuracy of 96.13% (κ = 0.95), enabling not only the accurate distinction of wetland types such as estuarine waters, aquaculture ponds, and reservoir ponds, but also precise delineation of the transition zones between estuarine and riverine systems. The spatial pattern of wetlands on Hainan Island revealed in this study is characterized by coastal concentration, greater abundance in the east than the west, artificial wetland clustering, and fragmentation of natural wetland types. These patterns reflect the island's ecological heterogeneity and the significant influence of anthropogenic activities. The results provide a reliable spatial dataset for wetland monitoring, ecological protection, and blue carbon stock estimation in tropical island environments. Furthermore, this framework lays a practical and methodological foundation for the future development of automated, semantic-level wetland mapping. By integrating hyperspectral, LiDAR, SAR time-series data, and object-oriented deep learning algorithms, future research can focus on advancing toward species-level or functional group-level wetland classification and long-term dynamic ecosystem monitoring.

Data availability statement

The raw data supporting the conclusions of this article will be made available by the authors, without undue reservation.

Ethics statement

Written informed consent was obtained from the individual(s) for the publication of any identifiable images or data included in this article.

Author contributions

XZ: Investigation, Methodology, Resources, Software, Writing – original draft, Writing – review & editing. JL: Investigation, Validation, Writing – original draft. SL: Project administration, Writing – review & editing. JY: Data curation, Writing – original draft. KD: Investigation, Writing – original draft. WD: Project administration, Supervision, Writing – review & editing. ZC:

Formal analysis, Investigation, Writing – original draft. FL: Data curation, Investigation, Writing – review & editing.

Conflict of interest

The authors declare that the research was conducted in the absence of any commercial or financial relationships that could be construed as a potential conflict of interest.

Generative AI statement

The author(s) declare that no Generative AI was used in the creation of this manuscript.

Any alternative text (alt text) provided alongside figures in this article has been generated by Frontiers with the support of artificial intelligence and reasonable efforts have been made to ensure accuracy, including review by the authors wherever possible. If you identify any issues, please contact us.

Publisher's note

All claims expressed in this article are solely those of the authors and do not necessarily represent those of their affiliated organizations, or those of the publisher, the editors and the reviewers. Any product that may be evaluated in this article, or claim that may be made by its manufacturer, is not guaranteed or endorsed by the publisher.

References

Adamus, P. (2013). *Wetland functions: not only about size* Vol. 35 (National Wetlands Newsletter), 18–25.

Anonymous (2020). Wetland monitoring using SAR data: A meta-analysis and comprehensive review. *Remote Sens.* 12, 2190. doi: 10.3390/rs12142190

Bartholomé, E., and Belward, A. S. (2005). GLC2000: a new approach to global land cover mapping from Earth observation data. *Int. J. Remote Sens.* 26, 1959–1977. doi: 10.1080/01431160412331291297

Bartold, M., Kluczek, M., and Dąbrowska-Zielińska, K. (2025). An automated approach for updating land cover change maps using satellite imagery. *Economics Environ.* 92, 810–810. doi: 10.34659/eis.2025.92.1.810

Bo, M., Jing-Ling, L., Kun, B., and Bin, S. (2020). Methodologies and management framework for restoration of wetland hydrologic connectivity: a synthesis. *Integrated Environ. Assess. Manage.* 16, 438–451. doi: 10.1002/ieam.4256

Claverie, M., Ju, J., Masek, J. G., and Dungan, J. L. (2018). The Harmonized Landsat and Sentinel-2 surface reflectance data set. *Remote Sens. Environ.* 219, 145–161. doi: 10.1016/j.rse.2018.09.002

Dabrowska-Zielinska, K., Bartold, M., and Gurdak, R. (2016). POLWET—System for new space-based products for wetlands under RAMSAR Convention. *Geoinf. Issues* 8, 25–35. doi: 10.34867/gi.2016.3

Dang, A. T. N., Kumar, L., Reid, M., and Nguyen, H. (2021). Remote sensing approach for monitoring coastal wetland in the mekong delta, Vietnam: change trends and their driving forces. *Remote Sens.* 13, 3359. doi: 10.3390/rs13173359

Dehua Mao, H. Y., Wang, Z., Song, K., Thompson, J. R., and Flower, R. J. (2022). Reverse the hidden loss of China's wetlands. *Science* 376, 1061. doi: 10.1126/science.adc88

Dronova, I. (2015). Object-based image analysis in wetland research: A review. *Remote Sens.* 7, 6380–6413. doi: 10.3390/rs70506380

Geng, Z., Jiang, W., Peng, K., Deng, Y., and Wang, X. (2023). Wetland mapping and landscape analysis for supporting international wetland cities: case studies in Nanchang City and Wuhan City. *IEEE J. Selected Topics Appl. Earth Observations Remote Sens.* 16, 1–14. doi: 10.1029/2023GL104642

Gong, P., Niu, Z., Cheng, X., Zhao, K., Zhou, D., Guo, J., et al. (2010). China's wetland change, (1990–2000) determined by remote sensing. *Sci. China-Earth Sci.* 53, 1036–1042. doi: 10.1007/s11430-010-4002-3

Gong, P., Wang, J., Yu, L., Zhao, Y., Zhao, Y., Liang, L., et al. (2013). Finer resolution observation and monitoring of global land cover: first mapping results with Landsat TM and ETM+ data. *Int. J. Remote Sens.* 34, 2607–2654. doi: 10.1080/01431161.2012.748992

Guo, M., Li, J., Sheng, C., Xu, J., and Wu, L. (2017). A review of wetland remote sensing. *Sensors* 17, 777. doi: 10.3390/s17040777

Guzinski, R. (2019). *GlobWetland africa toolbox: implementing EO-based wetland monitoring capacity in africa.* Germany: Copernicus Publications.

Hamid, J. M.M., Gill, E. W., and Mohammadimanesh, F. (2024). nhancing wetland mapping: integrating sentinel-1/2, GEDI data, and google earth engine. *Sensors* 24, 1651. doi: 10.3390/s24051651

Heimann, D. C., Femmer, S. R., Geological, S., and Missouri. Division of Environmental Q (1998). *Water quality, hydrology, and invertebrate communities of three remnant wetlands in Missouri 1995-97* (Rolla, Missouri: U.S: Department of the Interior, U.S. Geological Survey).

Henderson, F., and Lewis, A. (2008). Radar detection of wetland ecosystems: a review. *Int. J. Remote Sens.* 29, 5809–5835. doi: 10.1080/01431160801958405

Hou, D., Wang, S., Tian, X., and Xing, H. (2022). An attention-enhanced end-to-end discriminative network with multiscale feature learning for remote sensing image retrieval. *IEEE J. Selected Topics Appl. Earth Observations Remote Sens.* 15, 8245–8255. doi: 10.1109/JSTARS.2022.3208107

Hu, S., Niu, Z., Chen, Y., Li, L., and Zhang, H. (2017). Global wetlands: Potential distribution, wetland loss, and status. *Sci. Of Total Environ.* 586, 319–327. doi: 10.1016/j.scitotenv.2017.02.001

Igwe, V., Salehi, B., and Mahdianpari, M. (2022). STATE-WIDE WETLAND INVENTORY MAP OF MINNESOTA USING MULTI-SOURCE AND MULTI-TEMPORALREMOTE SENSING DATA. *ISPRS Ann. Photogrammetry Remote Sens. Spatial Inf. Sci.* V-3-2022, 411–416. doi: 10.5194/isprs-annals-V-3-2022-411-2022

Jamali, A., Roy, S. K., and Ghamisi, P. (2023). WetMapFormer: A unified deep CNN and vision transformer for complex wetland mapping. *Int. J. Appl. Earth Observation Geoinformation* 120, 103333. doi: 10.1016/j.jag.2023.103333

Jia, M., Wang, Z., Li, L., Song, K., Ren, C., Liu, B., et al. (2014). Mapping China's mangroves based on an object-oriented classification of Landsat imagery. *Wetlands* 34, 277–283. doi: 10.1007/s13157-013-0449-2

Jia, M., Wang, Z., Wang, C., Mao, D., and Zhang, Y. (2019). A new vegetation index to detect periodically submerged mangrove forest using single-tide Sentinel-2 imagery. *Remote Sens.* 11, 2043. doi: 10.3390/rs11172043

Jia, M., Wang, Z., Zhang, Y., Mao, D., and Wang, C. (2018). Monitoring loss and recovery of mangrove forests during 42 years: The achievements of mangrove conservation in China. *Int. J. Appl. Earth Observation Geoinformation* 73, 535–545. doi: 10.1016/j.jag.2018.07.025

Liu, M., and Hu, D. (2019). Response of wetland evapotranspiration to land use/cover change and climate change in liaohe river delta, China. *Water* 11, 955. doi: 10.3390/w11050955

Loveland, T. R., Reed, B. C., Brown, J. F., Ohlen, D. O., Zhu, Z., Yang, L., et al. (2000). Development of a global land cover characteristics database and IGBP DISCover from 1 km AVHRR data. *Int. J. Remote Sens.* 21, 1303–1330. doi: 10.1080/014311600210191

Mahdianpari, M., Granger, J. E., Mohammadimanesh, F., Salehi, B., Brisco, B., Homayouni, S., et al. (2020). Meta-analysis of wetland classification using remote sensing: A systematic review of a 40-year trend in north america. *Remote Sens.* 12, 1882. doi: 10.3390/rs12111882

Mao, D., Liu, M., Wang, Z., Li, L., Man, W., Jia, M., et al. (2019). Rapid invasion of spartina alterniflora in the coastal zone of mainland China: spatiotemporal patterns and human prevention. *Sensors* 19. doi: 10.3390/s19102308

Mao, D., Luo, L., Wang, Z., Wilson, M., Zeng, Y., Wu, B., et al. (2018a). Conversions between natural wetlands and farmland in China: A multiscale geospatial analysis. *Sci. Of Total Environ.* 634, 550–560. doi: 10.1016/j.scitotenv.2018.04.009

Mao, D., Wang, Z., Du, B., Li, L., Tian, Y., Jia, M., et al. (2020). National wetland mapping in China: A new product resulting from object-based and hierarchical classification of Landsat 8 OLI images. *ISPRS J. Photogrammetry Remote Sens.* 164, 11–25. doi: 10.1016/j.isprsjprs.2020.03.020

Mao, D., Wang, Z., Wu, J., Wu, B., Zeng, Y., Song, K., et al. (2018b). China's wetlands loss to urban expansion. *Land Degradation Dev.* 29, 2644–2657. doi: 10.1002/ldr.2939

Mitsch, W. J., Bernal, B., Nahlik, A. M., Mander, Ü., Zhang, L., Anderson, C. J., et al. (2013). Wetlands, carbon, and climate change. *Landscape Ecol.* 28, 583–597. doi: 10.1007/s10980-012-9758-8

Murray, N. J., Phinn, S. R., Dewitt, M., Ferrari, R., Johnston, R., Lyons, M. B., et al. (2019). The global distribution and trajectory of tidal flats. *Nature* 565, 222–225. doi: 10.1038/s41586-018-0805-8

Onojeghuo, A. O., Onojeghuo, A. R., Cotton, M., Potter, J., and Jones, B. (2021). Wetland mapping with multi-temporal sentinel-1 & -2 imagery, (2017–2020) and LiDAR data in the grassland natural region of alberta. *GIScience Remote Sens.* 58, 999–1021. doi: 10.1080/15481603.2021.1952541

Poiani, K. A., Johnson, W. C., Swanson, G. A., and Winter, T. C. (1996). Climate change and northern prairie wetlands: Simulations of long-term dynamics. *Limnology Oceanography* 41, 871–881. doi: 10.4319/lo.1996.41.5.0871

Pouliot, D., Latifovic, R., Pasher, J., and Duffe, J. (2019). Assessment of convolution neural networks for wetland mapping with landsat in the central canadian boreal forest region. *Remote Sens.* 11, 772. doi: 10.3390/rs11070772

Ren, C., Wang, Z., Zhang, Y., Zhang, B., Chen, L., Xi, Y., et al. (2019). Rapid expansion of coastal aquaculture ponds in China from Landsat observations during 1984–2016. *Int. J. Appl. Earth Observation Geoinformation* 82, 101902. doi: 10.1016/j.jag.2019.101902

Salimi, S., Almuktar, S. A. A. A. N., and Scholz, M. (2021). Impact of climate change on wetland ecosystems: A critical review of experimental wetlands. *J. Environ. Manage.* 286, 112160. doi: 10.1016/j.jenvman.2021.112160

Suzhen Yang, Y. W., Fang, Q., Elliott, M., Ikhumhen, H. O., Liu, Z., and Meilana, L. (2022). The transformation of 40-year coastal wetland policies in China: network analysis and text analysis. *Environ. Sci. Technol.* 56, 15251–15260. doi: 10.1021/acs.est.2c04683

Tickner, D., Opperman, J. J., Abell, R., Acreman, M., Arthington, A. H., Bunn, S. E., et al. (2020). Bending the curve of global freshwater biodiversity loss: an emergency recovery plan. *BioScience* 70, 330–342. doi: 10.1093/biosci/biaa002

UNEP-DHI (2024). *Global Wetland Watch: A system for global monitoring of wetlands.* Available online at: Available at: https://www.globalwetlandwatch.org.

Wang, M., Mao, D., Wang, Y., Xiao, X., Xiang, H., Feng, K., et al. (2023). Wetland mapping in East Asia by two-stage object-based Random Forest and hierarchical decision tree algorithms on Sentinel-1/2 images. *Remote Sens. Environ.* 297, 113793. doi: 10.1016/j.rse.2023.113793

Wang, Z., Wu, J., Madden, M., and Mao, D. (2012). China's wetlands: conservation plans and policy impacts. *Ambio* 41, 782–786. doi: 10.1007/s13280-012-0280-7

Weise, K., Höfer, R., Franke, J., Guelmami, A., Simonson, W., Muro, J., et al. (2020). Wetland extent tools for SDG 6.6.1 reporting from the Satellite-based Wetland Observation Service (SWOS). *Remote Sens. Environ.* 247, 111892. doi: 10.1016/j.rse.2020.111892

Whalen, S. C. (2005). Biogeochemistry of methane exchange between natural wetlands and the atmosphere. *Environ. Eng. Sci.* 22, 73–94. doi: 10.1089/ees.2005.22.73

Xing, H., Niu, J., Feng, Y., Hou, D., Wang, Y., and Wang, Z. (2023). A coastal wetlands mapping approach of Yellow River Delta with a hierarchical classification and optimal feature selection framework. *CATENA* 223, 106897. doi: 10.1016/j.catena.2022.106897

Xing, H., Zhu, L., Feng, Y., Wang, W., Hou, D., Meng, F., et al. (2021). An adaptive change threshold selection method based on land cover posterior probability and spatial neighborhood information. *IEEE J. Selected Topics Appl. Earth Observations Remote Sens.* 14, 1. doi: 10.1109/JSTARS.2021.3124491

Xu, X., Chen, M., Yang, G., Jiang, B., and Zhang, J. (2020). Wetland ecosystem services research: A critical review. *Global Ecol. Conserv.* 22, e01027. doi: 10.1016/j.gecco.2020.e01027

Zedler, J. B., and Kercher, S. (2005). WETLAND RESOURCES: status, trends, ecosystem services, and restorability. *Annu. Rev. Environ. Resour.* 30, 39–74. doi: 10.1146/annurev.energy.30.050504.144248

Zhang, X., Liu, L., Zhao, T., Chen, X., Lin, S., Wang, J., et al. (2023). GWL_FCS30: a global 30 m wetland map with a fine classification system using multi-sourced and time-series remote sensing imagery in 2020. *Earth System Sci. Data* 15, 265–293. doi: 10.5194/essd-15-265-2023

Zhi, L., Gou, M., Li, X., Bai, J., Cui, B., Zhang, Q., et al. (2022). Effects of sea level rise on land use and ecosystem services in the liaohe delta. *Water* 14, 841. doi: 10.3390/w14060841

Zhu, L., Xing, H., and Hou, D. (2022). Analysis of carbon emissions from land cover change during 2000 to 2020 in Shandong Province, China. *Sci. Rep.* 12, 1–12. doi: 10.1038/s41598-022-12080-0